Design and Characterization of a Wave Energy Converter Array Experimental Test Platform

by

Penelope Herrero-Marques

Submitted to the Department of Mechanical Engineering
in partial fulfillment of the requirements for the degree of

BACHELOR OF SCIENCE IN MECHANICAL ENGINEERING

at the

MASSACHUSETTS INSTITUTE OF TECHNOLOGY

May 2024

Authored by: Penelope Herrero-Marques
Department of Mechanical Engineering
May 10, 2024

Certified by: Dick K.P. Yue
Philip J. Solondz Professor of Engineering
Professor of Mechanical & Ocean Engineering, Thesis Supervisor

Accepted by: Kenneth Kamrin
Associate Professor of Mechanical Engineering
Undergraduate Officer, Department of Mechanical Engineering

Design and Characterization of a Wave Energy Converter Array Experimental Test Platform

by

Penelope Herrero-Marques

Submitted to the Department of Mechanical Engineering
on May 10, 2024 in partial fulfillment of the requirements for the degree of

BACHELOR OF SCIENCE IN MECHANICAL ENGINEERING

ABSTRACT

Wave energy is a promising source of renewable energy that has the potential to play a significant role in the global transition towards sustainable energy. Unlike other forms of renewable energy, wave energy is not dependent on weather patterns or daylight hours, making it a reliable and consistent source of energy. As the demand for clean energy continues to grow, wave energy can provide a valuable contribution to the global energy mix, helping to reduce greenhouse gas emissions and mitigate the negative impacts of climate change. Wave energy is harvested by wave energy converters—devices that convert the kinetic energy of ocean waves into electrical energy. Wave energy converter (WEC) arrays consist of multiple individual WEC devices that are arranged in a specific pattern. The arrangement of the devices within the array is designed to optimize their performance and reduce their negative effects on the surrounding environment. Developing reliable models of WEC array performance and optimal array configurations is critical to advancing research in this exciting field. This thesis details the design and validation of a test rig for experimentally testing wave energy converter array performance in the MIT Building 48 tow tank. The test rig features a novel magnetic damper that was designed and characterized to uniquely suit the conditions of the tow tank. The final test rig is capable of measuring the power captured by oscillating buoys as a function buoy shape, mass, and damping provided. Beyond facilitating hydrodynamics research, the test platform will be a valuable educational resource for classes such as Hydrodynamics that incorporate laboratory components. Its functionality will allow students to explore firsthand the principles of wave energy conversion, buoy dynamics, and the impact of various design parameters on energy capture. By providing hands-on experience, the test rig will enhance learning outcomes and cultivate a deeper understanding of renewable ocean energy technologies.

Thesis supervisor: Dick K.P. Yue
Title: Philip J. Solondz Professor of Engineering
Professor of Mechanical & Ocean Engineering

Acknowledgments

I would like to offer my deepest gratitude to Dr. Grgur Tokić and Prof. Dick K.P. Yue for guiding me through this research project and providing me with all of the tools I needed to succeed. Their patience and grace was invaluable and I truly could not have done it without them. Thank you for helping me explore my passion for renewable energy technologies and for helping me grow to become a better engineer.

Contents

List of Figures

Chapter 1

Introduction

Wave energy is a promising source of renewable energy that has the potential to play a significant role in the global transition towards sustainable energy. Unlike other forms of renewable energy, wave energy is not dependent on weather patterns or daylight hours, making it a reliable and consistent source of energy. As the demand for clean energy continues to grow, wave energy can provide a valuable contribution to the global energy mix, helping to reduce greenhouse gas emissions and mitigate the negative impacts of climate change.

Wave energy is harvested by wave energy converters—devices that convert the kinetic energy of ocean waves into electrical energy. Wave energy converter (WEC) arrays consist of multiple individual WEC devices that are arranged in a specific pattern. The arrangement of the devices within the array is designed to optimize their performance and reduce their negative effects on the surrounding environment. Developing reliable models of WEC array performance and optimal array configurations is critical to advancing research in this exciting field.

Figure 1.1: Tow Tank in MIT Building 48.

The aim of this research project is to design a test rig that will allow WEC array performance to be experimentally tested in the MIT Building 48 Tow Tank, shown in Figure 1.1.

This testing platform will be capable of measuring the power captured by oscillating buoys as a function buoy shape, mass, and damping provided.

Beyond facilitating hydrodynamics research, the test platform will be a valuable educational resource for classes such as 2.20 Hydrodynamics that incorporate laboratory components. Its functionality will allow students to explore firsthand the principles of wave energy conversion, buoy dynamics, and the impact of various design parameters on energy capture. By providing hands-on experience, the test rig will enhance learning outcomes and cultivate a deeper understanding of renewable ocean energy technologies.

1.1 Experimental Setup

The test platform will simulate an infinite array of WEC buoys in the Building 48 tow tank. This can be achieved using a singular WEC buoy and exploiting the tank's boundary conditions to virtually reflect the buoy across the tank's walls. The principle behind this method relies on the interaction between individual WEC buoys in an array and the incoming wave field. By employing appropriate boundary conditions, such as wave reflection, the tow tank can effectively mimic the effects of multiple buoys in an array.

When a wave encounters the WEC buoy in the tow tank, it causes the buoy to oscillate or move in response to the wave's energy. To simulate the presence of neighboring buoys, the tank's boundary acts as a virtual reflection surface. When the buoy reaches the tank's wall, the reflected wave from the wall creates a similar response in the buoy as if it were interacting with another nearby buoy. Figure 1.2 shows this phenomenon. This method effectively creates a periodic boundary condition, where the behavior of the single WEC buoy is representative of an infinite array of buoys. By carefully adjusting the buoy dimensions and wave characteristics, we can study the collective behavior and performance of WEC arrays in a controlled laboratory environment.

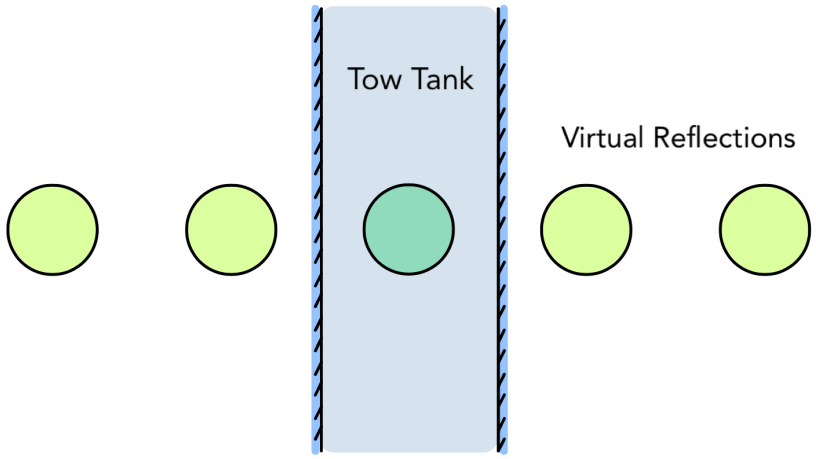

Figure 1.2: Top view of simulated infinite WEC array.

For a body j in a WEC array oscillating with a complex amplitude X_j, the mean extracted power P_j can be expressed as

$$P_j(\omega) = \frac{1}{2}\omega^2 b_{PTO}|X_j|^2 \tag{1.1}$$

where b_{PTO} is the power take-off device damping rate [1]. A damper will be used to replicate a linear power take-off device (PTO), which is the component in wave energy converters that converts the kinetic energy of the buoy motion into another, more useful, form. In a linear PTO, the damping rate is the constant of proportionality between buoy velocity and force exerted by the PTO. Once b_{PTO} is known, a position measurement is able to provide us with all other information needed to determine the power extracted by the WEC. As such, the test platform requires a continuous buoy positional measurement as well as a known damping rate on the order of 10 N/m/s. A variable damping rate would allow for increased test platform flexibility as well as for experimentally testing the effect of damping on WEC array performance.

Chapter 2

Test Platform Design

This chapter presents the design of the test platform developed for evaluating the performance of wave energy converters (WECs) in a tow tank. It details the functional requirements critical to ensuring accurate and reliable measurements. The discussion encompasses the construction of the buoy, the integration of precise instrumentation, and the application of linear damping mechanisms. These elements collectively form the foundation for the rigorous assessment of WEC performance, providing essential insights for subsequent experimental investigations.

2.1 Functional Requirements

The test platform requirements can be narrowed down to three key objectives:

- Constrain a buoy to heaving motion
- Continuously measure and record buoy position
- Provide variable, linear damping on the order of 10 N/m/s

The following sections will cover how each of these requirements were approached and ultimately met.

2.2 Buoy

We begin with the first design requirement: constraining a buoy to heaving motion. To do this, we must first have a buoy to work with! For simplicity and cost-effectiveness, a 5-gallon Home Depot bucket was selected as the foundation for a truncated vertical cylinder buoy. To connect the buoy to the test rig, we decided to use a 1.5" 80/20 aluminum extrusion mounted vertically upright in the center of the bucket. The 80/20 extrusion was chosen due to its strength and compatibility with off-the-shelf 80/20 linear bearings. These linear bearings are what will constrain the buoy to heaving motion only. The connection between the bucket and the aluminum extrusion needed to be secure enough to withstand hydrodynamic wave forces while remaining upright and fixed to the buoy. Additionally, any internal bucket

structure needed to allow for easy filling of the bucket with sand. This would be important for controlling submerged cylinder depths in future experiments.

The internal bucket structure was made with 0.25" laser-cut plywood and 1" x 2" lumber. It was attached to the bucket using wood screws and all attachment points were sealed with silicone for waterproofing. Cutouts were included in the plywood to facilitate easy addition and removal of sand. The 80/20 aluminum extrusion was reinforced by two 0.25" plywood plates to ensure it remained perpendicular to the bottom of the bucket. Lastly, two aluminum L-brackets were used to attach the 80/20 extrusion to the internal wooden structure. The final buoy is shown in Figure 2.1.

(a) Internal buoy structure

(b) Fully assembled buoy with 80/20 extrusion

Figure 2.1: Final Buoy Configuration.

2.3 Instrumentation

As specified by the second functional requirement, the instrumentation on board must continuously measure and record buoy position. Some additional goals include:

- Sensor resolution finer than $\pm$ 2 mm
- Sensing range between 0.1 m and 1 m
- Sampling frequency greater than 100 Hz

We initially considered using an accelerometer to obtain position data, but were dissuaded by the drift errors that can occur due to the integration of noise when integrating acceleration to obtain position. We concluded that measuring position directly would lead to cleaner measurements that were less susceptible to drift.

Another important consideration was the environment in which these sensors would be operating—a tow tank. It was crucial that the sensing mechanism we chose was not susceptible to ambient light reflections, surface reflectivity, or humidity. For these reasons, we decided to avoid optical, IR, and ultrasonic position sensors if possible.

String potentiometers, also called draw wire sensors, are linear position sensors that are physically attached to the positional object of interest. They utilize a flexible cable, a spring-loaded spool, and a rotational sensor to detect changes in linear position. After a cable is attached to the object of interest, a spring-loaded spool converts any linear motion into a rotational displacement that is detected by the rotary sensor. Figure 2.2 illustrates the components of string potentiometers in greater detail. String potentiometers offer unique advantages in our situation. Since a cable would be physically attached to the heaving buoy, the position measurement would remain unaffected by splashes of water, surface reflections, humidity, and any other environmental factors. Due to simplicity and robustness, a string potentiometer was ultimately selected.

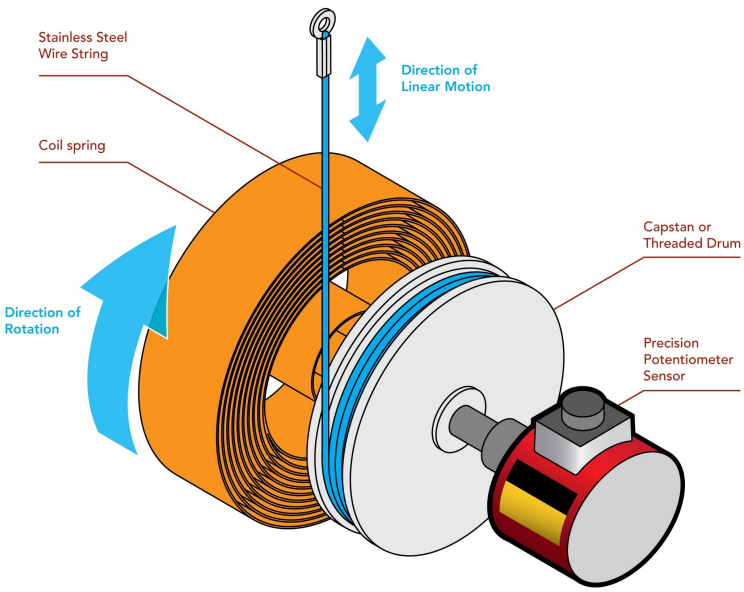

Figure 2.2: String Potentiometer Architecture [2]

After an unsuccessful search for a suitable and low-cost commercial string potentiometer, a simple string potentiometer was crafted from a tape measure coil spring, a 10-turn 10kΩ potentiometer, and 3D-printed housing. The potentiometer produced an analog output which was collected with an Arduino UNO. The Arduino UNO features a 10-bit analog-to-digital converter with a maximum sampling rate of 15kHz. With a maximum sampling rate well above 100 Hz, the third sub-design requirement was met.

Before assembling the string potentiometer, a theoretical analysis was performed to determine the anticipated sensor resolution and measurement range. This was done to ensure that the first and second sub-design requirements were met: achieving a sensor resolution greater than ± 2 mm and a sensing range between 0.1 m to 1 m.

The tape measure spool diameter was 44.6 mm, meaning that each full revolution corresponded to $L = (\pi)(44.6\,\text{mm}) = 140.04\,\text{mm}$ of linear motion. A 10-turn potentiometer therefore has a maximum sensing range $(10)(140.04\,\text{mm}) = 1400.04\,\text{mm} = 1.4\,\text{m}$. This exceeds the second design requirement of achieving a sensing range of 0 m to 1.4 m. Lastly, the Arduino's 10-bit analog-to-digital converter provides $2^{10} = 1024$ unique steps. For a 10-turn potentiometer, this means there are $(1024)/(10) = 102.4$ steps per revolution. A linear distance of 140.04 mm per revolution therefore gives a sensor resolution of (140.04 mm)/(102.4 steps) = ± 1.37 mm. This once again exceeds the design requirement of ± 2.5 mm sensor resolution.

After confirming that the design requirements would be satisfied with the current sensor configuration, the string potentiometer was assembled. The final string potentiometer is shown in Figure 2.3. The black and white housing was made from 3D printed PLA, the blue potentiometer can be seen on top, and the draw wire is on the bottom right. Once assembled, the sensor resolution was experimentally verified by displacing the string a fixed amount and recording the digital output. This was repeated several times and the results were then averaged together to find an experimental resolution of ± 1.41 mm. This confirmed the theoretical analysis was accurate and that the first design constraint was indeed met.

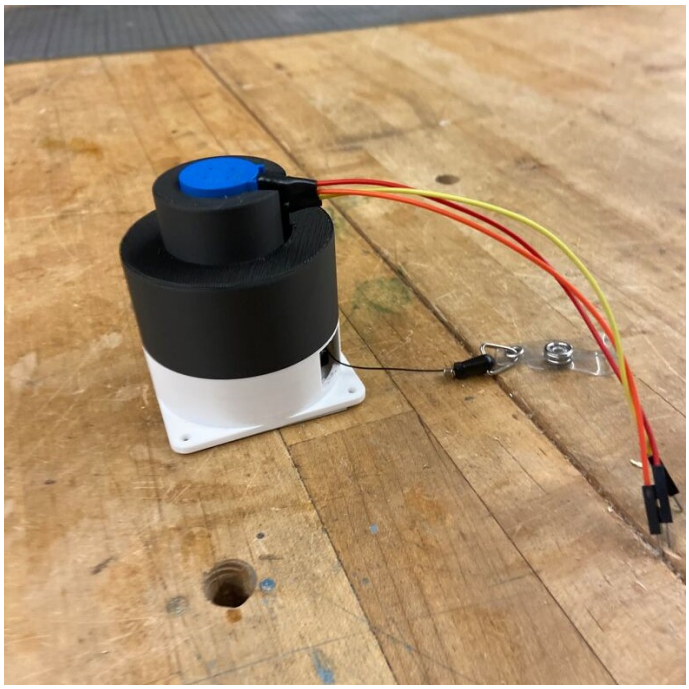

Figure 2.3: Final string potentiometer.

2.4 Damping

The final functional requirement specifies that the test rig must be able to provide variable, linear damping to the heaving buoys on the order of 10 N/m/s. This damper will replicate a linear power take-off device (PTO), which is the component in wave energy converters that converts the kinetic energy of the buoy motion into another, more useful, form. In a linear PTO, the damping rate is the constant of proportionality between buoy velocity and force exerted by the PTO. Being able to vary the damping rate provided allows for experimental testing of the various effects of buoy damping on overall array performance, as well as flexibility in the types of buoys compatible with the test rig.

Dampers can generally be classified into two configurations: linear and rotational. Before continuing, it is important to clarify that here we refer to a linear damper as a damper which acts on linear motion as opposed to rotational motion. Based on the previous work on this project, the initial plan was for the test rig to use a rotary damper whose moment arm attached to the heaving buoy with a combined linear-rotational joint, as can be seen in Figure 2.5. Most of the components needed for this configuration were already purchased, including a Kinetrol Model KD-A2-DD Rotary Dashpot (Figure 2.4). The Kinetrol dashpot was rated for variable damping between 1.13 to 11.3 Nm/rad/s and featured a 60° range of motion. The limited angular range of motion meant that the moment arm length would have to be adjusted according to the buoy's heaving amplitude to ensure that the 60° range was not exceeded. Additionally, the sliding pivot joint used to couple the rotational damper motion to the linear reciprocating motion of the buoy would change the moment arm length as the buoy heaves up and down. This creates a time-dependent effective buoy mass which further increases the complexity of the system.

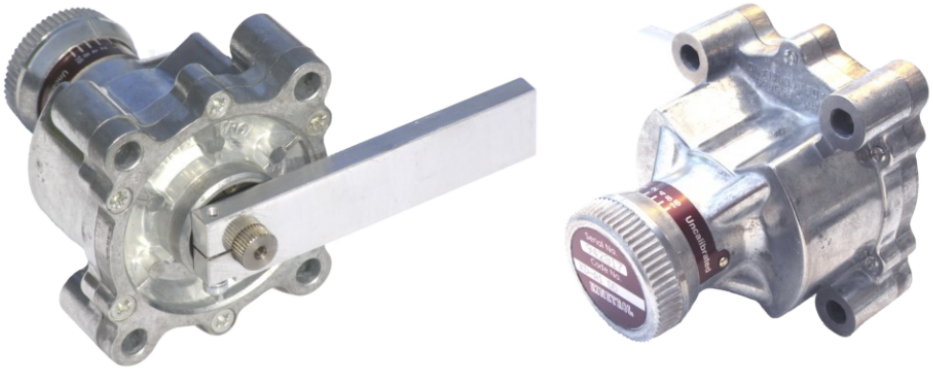

Figure 2.4: Kinetrol Rotary Dashpot, Model KD-A2-DD. [3]

Seeking to reduce complexity, we began to consider other system configurations. The straightforward alternative was using a linear damper. This would eliminate the need for a combined linear-rotational joint, meaning the buoy would have a constant effective mass. Figure 2.5 compares these two configurations. Due to the reduced design complexity and fewer degrees of freedom, the linear configuration emerged as the most suitable choice for our application.

The biggest considerations for the linear damper would be variable damping and stroke

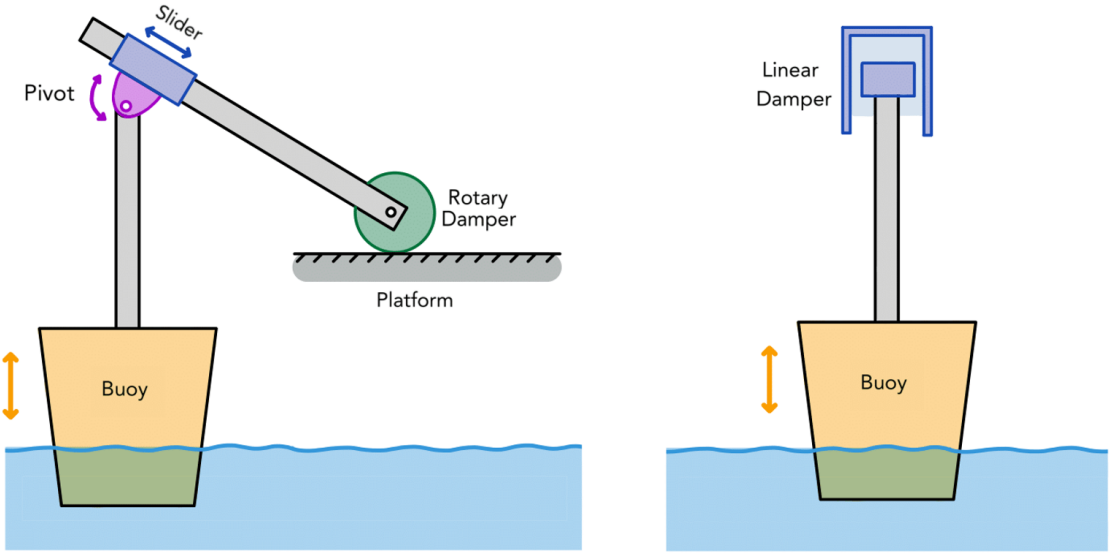

(a) Rotary Damping Configuration.

(b) Linear Damping Configuration.

Figure 2.5: Rotary vs. Linear Damping configurations.

length, which must be greater than the maximum heave amplitude. We were unable to find an off-the-shelf product with a large enough range of motion and decided to create our own solution. Chapter 3 discusses the design and validation of this damper.

Chapter 3

Linear Damper

This chapter focuses on the design and validation of a novel linear damper specifically suited for tow tank WEC experimentation. Magnetic damping was selected as the mechanism of choice, and governing equations were derived to inform the design process. The damper was built and subsequently characterized through experimental methods, including the use of a mass-spring-damper system and a series of free decay tests to measure the damping rate. Additionally, a linear damping rate vs. current relationship was established as a guide on how damping varies in response to current inputs. This analysis offers essential insights into the performance and optimization of the magnetic damper.

3.1 Magnetic Damping

Magnetic damping, also referred to as eddy current damping, is a phenomenon that occurs when a magnetic field travels through a non-magnetic electrical conductor. As the magnetic field moves through the conductor, circular eddy currents are induced in the conductive material. These circulating eddy currents generate an opposing magnetic field according to Lenz's Law. The opposing magnetic field causes the conductor to experience a drag force that opposes its motion. This force is directly proportional to the velocity of the conductive material, meaning that a magnetic damper can replicate a linear PTO. Figure 3.1 illustrates this phenomenon.

The damping rate of a magnetic damper can be adjusted by varying the strength of the magnetic field. This can be done with electromagnets, whose strength is proportional to the amount of current flowing through them, as opposed to permanent magnets that have a constant magnetic field. The variable current can be easily provided to the electromagnets by a benchtop power supply next to the test rig.

Magnetic damping is not reliant on a specific geometric configuration to function; it simply requires magnetic flux through a conductor. This design flexibility means that a magnetic damper could be uniquely adapted to the conditions of the tow tank. Due to this design flexibility and the ease of achieving variable damping, magnetic damping emerged as the most suitable damping mechanism for our application.

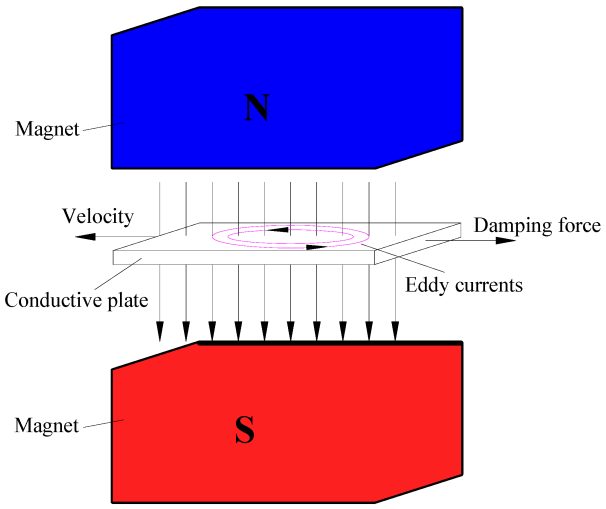

Figure 3.1: Eddy currents induced by a conductor moving through a magnetic field. [4]

3.2 Governing Equations

We begin by deriving the expression for magnetic damping rate. In [5], Heald derives the following closed-form expression for the magnitude of drag force produced by electromagnetic interaction in eddy current brakes assuming an infinite conductive plate

$$F_d = \alpha(\sigma\delta B_0^2 A)v, \tag{3.1}$$

where α is a dimensionless shape factor related to the pole shape of the magnet, σ is the conductivity of the metal, δ is the thickness of the conductor, B_0 is the field strength in the gap between the magnets, A is the area of the pole face of the magnet, and v is the relative velocity between the magnets and the conductor. The shape factor α is given by

$$\alpha = 1 - \frac{1}{2\pi}\left[4\arctan AR + AR\ln\left(1+\frac{1}{AR^2}\right) - \frac{1}{AR}\ln\left(1+AR^2\right)\right], \tag{3.2}$$

where $AR = l/w$ is the aspect ratio of the magnetic footprint.

From expression 3.1, it is clear that drag force is directly proportional to velocity, as expected. The damping coefficient can thus be expressed as

$$b = \alpha\sigma\delta B_0^2 A. \tag{3.3}$$

The parameters α, σ, δ, and A are related to the geometric configuration of the system. Field strength, B_0, is driven by electromagnet rating. Since most electromagnets on the market are rated by holding force, an expression relating magnetic holding force to magnetic field strength is needed. The mechanical force between two nearby magnetized surfaces can be calculated with the following expression [6]:

$$F = \frac{(B_0)^2 S}{2\mu_0}, \tag{3.4}$$

where B_0 is magnetic field strength in Teslas, S is the area of the magnetized surface, and μ_0 is the permeability of free space, which equals $4\pi \times 10^{-7}$ T·m/A. It is important to note that this expression is only valid for cases in which the air gap between the two surfaces is negligible compared to the area of the magnetized surfaces. To compensate for potential discrepancies caused by edge effects and the air gap, a safety factor of 1.5 was used when sourcing electromagnets.

3.3 Design

Having derived a working set of governing equations, we are now able to begin damper design. The side view of the general damper configuration is shown in Figure 3.2. Critical dimensions are labelled in gray.

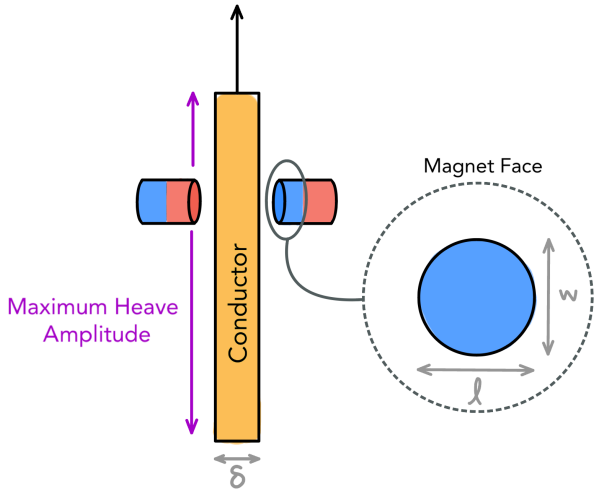

Figure 3.2: Magnetic Damper Configuration

We began with material selection. Metal conductivity, σ, was the most important material property to consider in order to maximize the damping rate. With the highest conductivity of any common engineering metal at 59.6×10^6 S/m, copper was the obvious choice [7]. After considering cost and weight, we settled on a copper thickness of $\delta = 3/8"$ (4.76 mm). For heave amplitude flexibility, we ordered a 24" long 110 copper bar with the understanding that it could always be trimmed down to a more suitable length if needed.

The most critical components of the design were the electromagnets. Using the material properties of copper, the system dimensions, and a desired damping rate of 10 Ns/m, Equation 3.3 was used to calculate required magnetic field strength for different off-the-shelf electromagnets. Equation 3.4 was then used to check if the theoretical magnetic field strength of said electromagnet was at minimum 1.5 times greater than the predicted magnetic field strength given by Equation 3.3. This process was repeated for a number of electromagnets until a suitable match was found. The Heyiarbeit 12V DC 1200N electromagnet, shown in Figure 3.3, satisfied all requirements, producing an approximate field strength of 0.387 Tesla when a field of 0.105 Tesla was required for its specific geometry. It is important to note that the 0.387 Tesla field strength is a generous approximation since field strength decreases

with distance cubed. Even with a small gap distance of 1/8" between the copper bar and magnet, the field strength will decay significantly. This is why it was important to build in safety factors into our design.

Figure 3.3: Heyiarbeit 12V DC 1200N Electromagnet [8]

After selecting the components of the damper, a simple frame was built from wood using a combination of 0.5" plywood and 1"x2" lumber. Wood was chosen due to its lightweight yet sturdy nature. Linear slide bearings were 3D printed and lubricated with WD-40 to guide the copper bar. The electromagnets were attached to the wooden frame using aluminum L-brackets. Different angles of the CAD model are shown in Figure 3.4. The black components are the 3D printed sliders and the white casing represents the wooden frame. In the 3/4 view and side view, a wooden panel is removed for increased internal visibility.

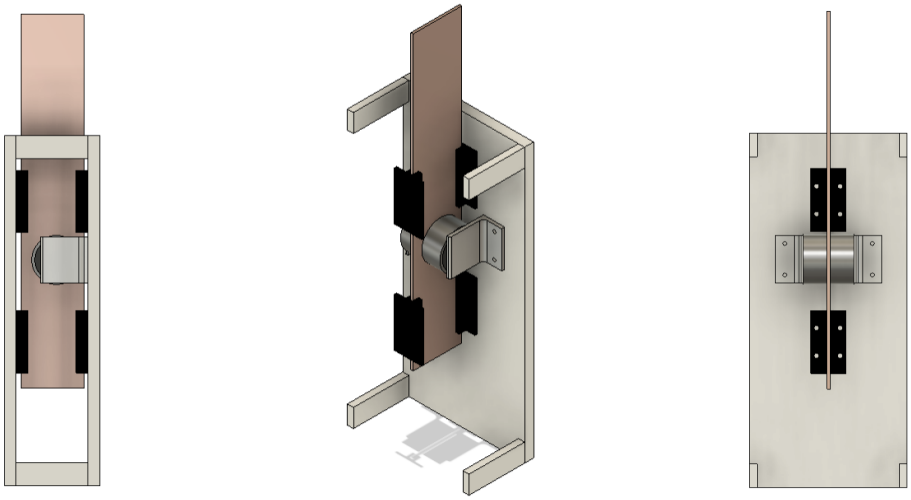

(a) Front View. (b) 3/4 view. (c) Side view.

Figure 3.4: Magnetic Damper CAD Models.

The completed damper is shown in Figure 3.5.

Figure 3.5: Finished Magnetic Damper.

3.4 Damper Characterization

As mentioned in the previous section, the governing equations used to design the magnetic damper were general approximations. As is often the case in magnetic design, it is usually simpler to make an informed guess and then extensively test the final design to determine where the modeling might have fallen short. With this approach in mind, a series of experiments were performed to characterize the damper. The ultimate goal of these experiments was to verify that the damping was linear and determine the relationship between current supplied to the electromagnets and the damping rate provided.

3.4.1 Methodology

To characterize the damper and test whether the desired damping rate could be achieved, we decided to build a simple mass-spring-damper and conduct a series of free decay tests. To convert the magnetic damper into a mass-spring-damper system, a spring was directly

attached to the copper plate, as can be seen in Figure 3.6. Two wooden posts were added to the top of the damper frame and an aluminum rod supported the spring.

Figure 3.6: Magnetic Damper converted into mass-spring-damper system.

A series of free decay tests were performed while varying magnetic field strength. The magnetic field strength was changed by adjusting the current supplied to the electromagnets with a benchtop power supply. In each test, the copper plate was displaced downward by 3" and then allowed to freely oscillate. The position of the copper plate was measured with the string potentiometer and recorded by an Arduino UNO at a sampling rate of 100 Hz. Three free decay tests were performed per current level. Nine discrete current levels were tested, ranging from 1.2 A to 3.3 A, for a total of 27 trials.

The positional data from the free decay tests was imported into MATLAB where a damped sinusoid of the form

$$x(t) = Ae^{-\lambda t} \sin(\omega_d t - \phi) \tag{3.5}$$

was fitted to the data using a least squares regression technique. Here, $\lambda = \frac{b}{2m}$ where b is the damping rate in N/m/s and m is the system mass in kilograms. Thus, from the sinusoid fit, the damping rate was determined for each trial.

3.4.2 Experimental Results

The selected spring had a spring constant of $k = 508$ N/m and the copper weighed 2.62 kg. Assuming a typical second-order mass-spring-damper system, the expected natural frequency would be

$$\omega_n = \sqrt{\frac{k}{m}} = \sqrt{\frac{508}{2.62}} = 13.92 \text{ rad/s} \tag{3.6}$$

The natural frequency served as a crucial benchmark for all trials. Ensuring that the damped sinusoid fits produced a consistent natural frequency was the initial indicator of the system's expected linear behavior. Figure 3.7 shows sample position data from the free decay trials for two different current levels with the theoretical response obtained by curve fitting overlaid. As expected, increasing the current produces a stronger magnetic field which leads to a greater amount of damping. The natural frequency found from curve fitting for all trials was 13.91 ± 0.01 rad/sec, confirming our system was behaving as expected.

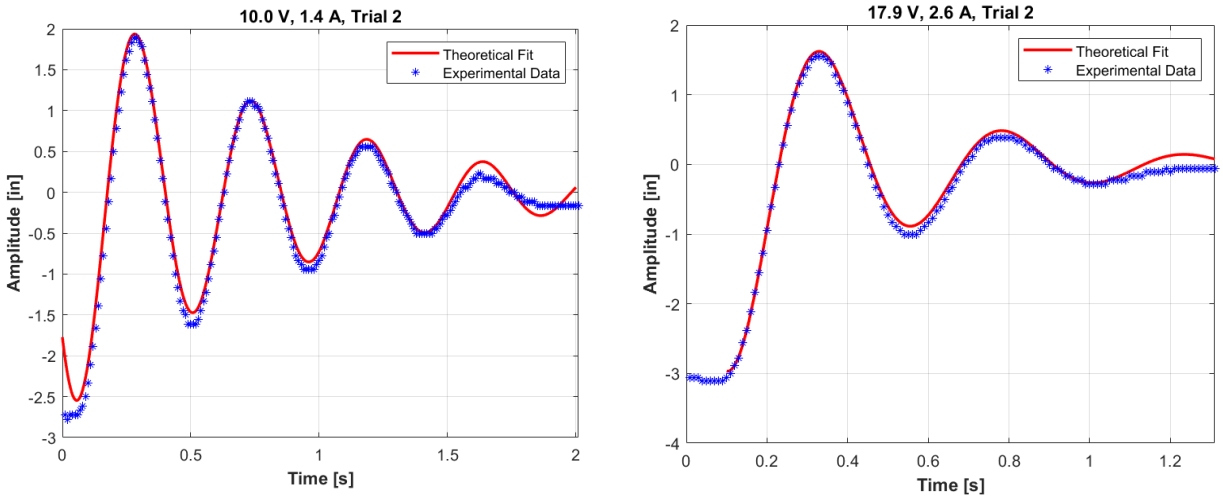

(a) 1.4 A

(b) 2.6 A

Figure 3.7: Free Decay Test Data.

As can be seen in Figure 3.7, nonlinear effects were present at amplitudes below 0.2" (5 mm). These nonlinear effects can largely be attributed to sensor discretization and frictional effects that occur at lower velocities. Since the buoy heaving amplitudes that will be tested almost always be greater than 0.2", these nonlinear effects should not affect damper performance in the town tank.

After analyzing all 27 trials, we could determine the relationship between current supplied to the electromagnets and the damping rate provided. To begin, we plotted all damping results against the current levels supplied to the electromagnets, shown in Figure 3.8.

As expected, the curve appeared to show a linear relationship between current provided and damping rate. As such, we performed a linear fit which can be seen in Figure 3.9. Note: error bars are present in this figure, however, due to the tight spread in some trials, some error bars are small and difficult to see. The resulting linear fit was $b = 6.765I - 3.056$,

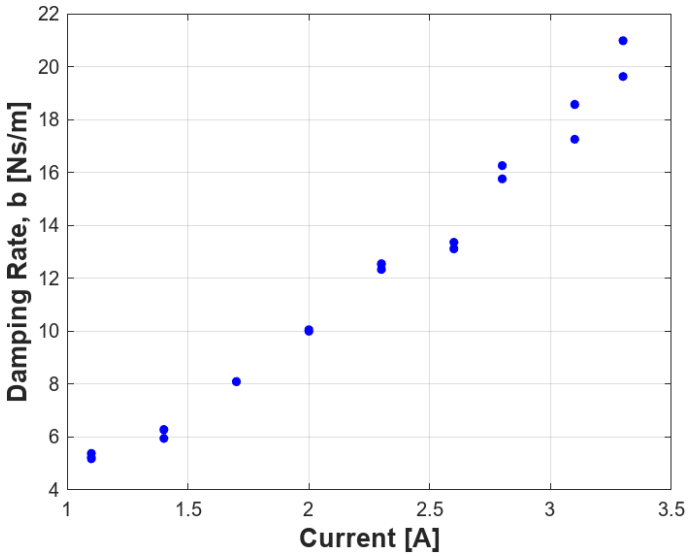

Figure 3.8: Damping Rate vs. Current Plot with all experimental data.

with uncertainties of 6.765 ± 0.456 $\frac{N/m/s}{A}$ and 3.056 ± 1.075 N/m/s. The slope of this linear fit is significantly less than the slope of 426 $\frac{N/m/s}{A}$ predicted by Equation 3.3 when assuming a magnetic field strength of 0.387 Tesla. However, it is on par with the slope of 10.47 $\frac{N/m/s}{A}$ predicted with a field strength of 0.1 Tesla. This confirms that, as expected, the predicted field strength of 0.387 Tesla was indeed an overestimate, highlighting the necessity of including a generous safety factor when selecting the electromagnets. Although there is a slight discrepancy between the linear fit and the experimental results at 2.6 A, the linear fit provides a useful guide on how damping varies in response to current inputs. This curve and the linear relation obtained will serve as a useful guide to test rig damping for future tow tank experiments.

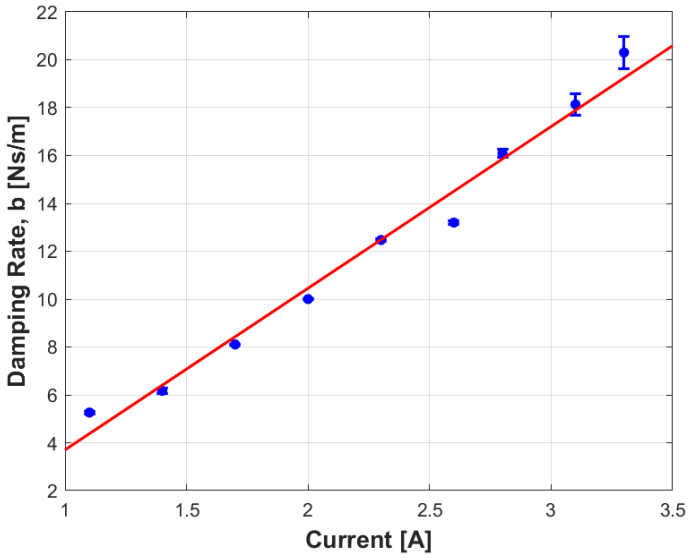

Figure 3.9: Damping Rate vs. Current Plot with linear fit superimposed.

The experimental data and subsequent analysis confirmed that the magnetic damper we constructed was capable of providing variable, linear damping between 5-20 N/m/s. While there were some nonlinear effects present at amplitudes less than 0.2", they were negligible at the heaving amplitudes that the test rig will handle. As such, the final functional requirement of the test rig was met.

Chapter 4

Conclusion

Throughout this thesis, we have detailed the design and validation of a test rig for experimentally testing wave energy converter array performance. The project successfully achieved the three core functional requirements:

- Constrain a buoy to heaving motion
- Continuously measure and record buoy position
- Provide variable, linear damping on the order of 10 N/m/s

We constructed a truncated vertical cylinder buoy with adjustable weight, allowing for precise control by adding or removing sand. An 80/20 aluminum extrusion was utilized to create a modular attachment point for future buoy iterations, ensuring scalability and ease of modification. Additionally, we developed a string potentiometer to continuously measure buoy position. This position sensor surpassed the required sensor resolution of $\pm$ 2.5mm, with an experimentally validated resolution of $\pm$ 1.41mm.

The newly built magnetic damper demonstrated the ability to provide linear damping between 5-20 N/m/s while accommodating a wide range of heave amplitudes, with a maximum allowable amplitude exceeding 12 inches. Characterization of the damper was conducted through the construction of a mass-spring-damper system and a series of free decay tests. A Damping Rate vs. Current curve was generated, revealing a linear functional relationship that enabled the adjustment of current input to achieve a desired level of damping ranging from 5 to 20 N/m/s.

While our test rig offers significant advancements in experimental testing for wave energy converter (WEC) performance, it also comes with certain limitations. One limitation is that the rig can only accommodate buoys with radiation damping between 5-20 N/m/s. Additionally, the inclusion of the copper plate and 80/20 extrusions adds unnecessary weight to the buoy, potentially affecting buoy dynamics and limiting the size of buoys compatible with the test rig. Another limitation is the lack of direct force measurement, which can be a key parameter for accurately measuring power extracted by the buoys, as well as other quantities of interest. Incorporating direct force measurement would provide valuable information currently missing from the experimental setup.

Future work involves integrating all sub-components and deploying the rig in the tow tank. Figure 4.1 illustrates the intended final design. The green platform represents the tow tank platform which the test rig will be mounted to. The design uses 80/20 aluminum extrusions to mount the magnetic damper and buoy to the platform while an 80/20 linear bearing constrains the buoy to heave-only motion.

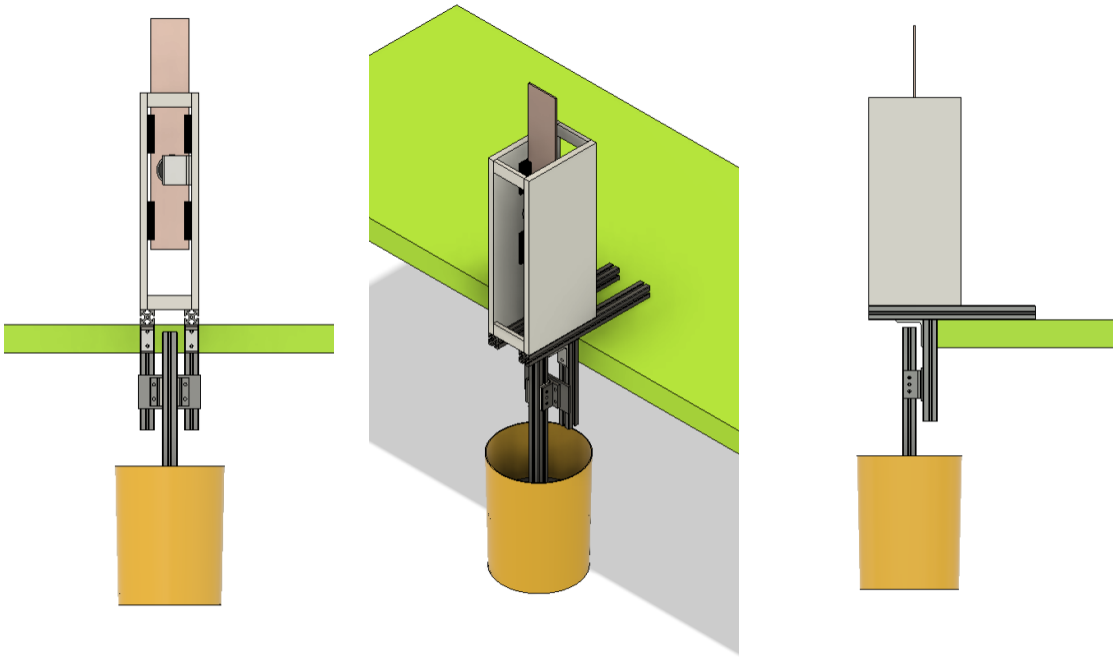

(a) Front view. (b) 3/4 view. (c) Side view.

Figure 4.1: Final Test Rig CAD Model.

Through this work, we contribute to the advancement of wave energy conversion technology, offering insights that can inform future research and development efforts. By bridging the gap between theoretical design and practical experimentation, we move closer to realizing the full potential of wave energy as a sustainable and renewable resource. Beyond facilitating hydrodynamics research, the test platform will be a valuable educational resource for classes such as Hydrodynamics that incorporate laboratory components. Its functionality will allow students to explore firsthand the principles of wave energy conversion, buoy dynamics, and the impact of various design parameters on energy capture. By providing hands-on experience, the test rig will enhance learning outcomes and cultivate a deeper understanding of renewable ocean energy technologies, thus inspiring the next generation of innovators in this field.

References

[1] G. Tokic and D. K. Yue, "Hydrodynamics of periodic wave energy converter arrays," *Jounral of Fluid Mechanics*, vol. 862, pp. 34–74, 2019. URL: doi:10.1017/jfm.2018.911.

[2] "What is a string potentiometer sensor?" Futek. (2024), URL: https://www.futek.com/string-potentiometer (visited on 04/23/2024).

[3] "Kinetrol model kd 60° vane dashpot," Kinetrol. (2022), URL: https://www.kinetrol.com/wp-content/uploads/2022/03/WEBDS204_DP_KD.pdf (visited on 06/13/2023).

[4] W. Wang, D. Dalton, X. Hua, X. Wang, Z. Chen, and G. Song, "Experimental study on vibration control of a submerged pipeline model by eddy current tuned mass damper," *Applied Sciences*, vol. 7, no. 10, 2017, ISSN: 2076-3417. DOI: 10.3390/app7100987. URL: https://www.mdpi.com/2076-3417/7/10/987.

[5] M. A. Heald, "Magnetic braking: Improved theory," *American Jounral of Physics*, vol. 56, pp. 521–522, 1988. URL: https://doi.org/10.1119/1.15570.

[6] F. Gram. "Magnetic fields and forces," Cuyahoga Community College. (2003), URL: http://instruct.tri-c.edu/fgram/web/Mdipole.htm (visited on 06/26/2023).

[7] "Electrical conductivity - elements and other materials," The Engineering ToolBox. (2008), URL: https://www.engineeringtoolbox.com/conductors-d_1381.html (visited on 06/26/2023).

[8] "Heyiarbeit 12v dc 1200n electric lifting magnet," Amazon. (2023), URL: https://www.amazon.com/Heyiarbeit-Electric-Electromagnet-Automation-Equipment/dp/B08Z39V9JD?ref_=ast_sto_dp&th=1 (visited on 06/30/2024).